

Article

Enhanced Electrochemical Performance of $\text{LiNi}_{1/3}\text{Co}_{1/3}\text{Mn}_{1/3}\text{O}_2$ at a High Cut-Off Voltage of 4.6 V by $\text{Li}_{1.3}\text{Al}_{0.3}\text{Ti}_{1.7}(\text{PO}_4)_3$ Coating

Ming Zhang ^{1,2}, Peng Zhang ^{1,*}, Weidong Wen ¹, Huanwen Wang ¹, Beibei He ¹, Yansheng Gong ¹, Jun Jin ¹ and Rui Wang ^{1,*} 

¹ Faculty of Materials Science and Chemistry, China University of Geosciences, Wuhan 430074, China

² Wuhan Institute of Marine Electric Propulsion, Wuhan 430064, China

* Correspondence: zp@cug.edu.cn (P.Z.); wangrui@cug.edu.cn (R.W.)

Abstract: At present, $\text{LiNi}_{1/3}\text{Co}_{1/3}\text{Mn}_{1/3}\text{O}_2$ (NCM) is a widely used material in the commercial market due to the easy control of the preparation process and usage environment. However, its capacity keeps fading when the cut-off voltage increases. In this research, an $\text{Li}_{1.3}\text{Al}_{0.3}\text{Ti}_{1.7}(\text{PO}_4)_3$ (LATP) coating method is proposed to improve the cycle performance of $\text{LiNi}_{1/3}\text{Co}_{1/3}\text{Mn}_{1/3}\text{O}_2$ at a high cut-off voltage of 4.6 V. The battery prepared with LATP-modified NCM exhibits an increased discharge capacity retention of 92.37% after 100 cycles at 0.2C (1C = 200 mA g⁻¹), while the bare NCM only presents 64.28%. Our results indicate that LATP-surface coating might be a useful method to increase the cycle stability of NCM and other high-capacity cathode materials.

Keywords: lithium-ion batteries; cathode; $\text{LiNi}_{1/3}\text{Co}_{1/3}\text{Mn}_{1/3}\text{O}_2$; $\text{Li}_{1.3}\text{Al}_{0.3}\text{Ti}_{1.7}(\text{PO}_4)_3$; surface modification



Citation: Zhang, M.; Zhang, P.; Wen, W.; Wang, H.; He, B.; Gong, Y.; Jin, J.; Wang, R. Enhanced Electrochemical Performance of $\text{LiNi}_{1/3}\text{Co}_{1/3}\text{Mn}_{1/3}\text{O}_2$ at a High Cut-Off Voltage of 4.6 V by $\text{Li}_{1.3}\text{Al}_{0.3}\text{Ti}_{1.7}(\text{PO}_4)_3$ Coating. *Coatings* **2022**, *12*, 1964. <https://doi.org/10.3390/coatings12121964>

Academic Editor: Ioannis V. Yentekakis

Received: 28 October 2022

Accepted: 11 December 2022

Published: 15 December 2022

Publisher's Note: MDPI stays neutral with regard to jurisdictional claims in published maps and institutional affiliations.



Copyright: © 2022 by the authors. Licensee MDPI, Basel, Switzerland. This article is an open access article distributed under the terms and conditions of the Creative Commons Attribution (CC BY) license (<https://creativecommons.org/licenses/by/4.0/>).

1. Introduction

Recently, the dramatic development of the automobile industry has put forward higher requirements for batteries with high specific energy densities. Cathode is an important component of lithium-ion batteries, and improving its electrochemical performance is one of the hot spots at present [1–3]. Typical cathode materials include α - NaFeO_2 -type LiCoO_2 and LiNiO_2 , spinel LiMn_2O_4 , and olivine LiFePO_4 [4]. Among them, LiCoO_2 is the first commercial cathode material, but the high cost of Co elements limits its applications in new electric vehicles [5–7]. In 1999, based on the study of layered binary cathode materials, Liu et al. first proposed to replace Ni in LiNiO_2 with Co and Mn to prepare $\text{LiNi}_{1-x-y}\text{Co}_x\text{Mn}_y\text{O}_2$ cathode materials [8]. This kind of material shows some advantages, such as low cost high specific capacity. Therefore, this type of ternary material is considered to be an important material to substitute commercial LiCoO_2 [9–12]. Currently, the elemental ratios of ternary materials used in industry are 111, 523, 622, and 811, among which NCM111(NCM) is a widely used material in the industry due to the easy control of the preparation process and usage environment [13,14]. However, compared with other ternary materials, the energy density of NCM material is still unsatisfactory and needs to be improved [15,16]. The easiest way to do so is to increase the cut-off voltage. Unfortunately, when the cut-off voltage reaches a certain value, the cathode electrolyte interphase (CEI) becomes unstable, and it continuously decomposes and regenerates in the charge and discharge cycles [17–20]. This continuous side reactions leads to increased internal resistance, which leads to poor battery performance.

Surface modification is a widely used and effective way to alleviate the surface side reactions of cathodes [21,22]. Huang et al. employed a one-step method and successfully coated carbon on the NCM surface [23]. This surface layer effectively enhanced the electron conductivity and inhibited the occurrence of side reactions between the cathode and electrolyte. Similarly, Wang et al. reported coating AlPO_4 on NCM by a chemical deposition method and improved the electrochemical performance [24]. Besides, several metal oxide

layers have been reported to improve the performance of NCM, such as Li_2MoO_4 [25], B_2O_3 [26], Al_2O_3 [27], Sb_2O_3 [28], and V_2O_5 [29], and they all show promising effects.

$\text{Li}_{1.3}\text{Al}_{0.3}\text{Ti}_{1.7}(\text{PO}_4)_3$ (LATP) is a lithium ionic conductor and considered to be a promising solid-state electrolyte in lithium batteries [30–32]. It is reported to be an effective layer on a LiCoO_2 surface to increase the electrochemical performance. The reason may be that it could protect the surface from the corrosion by HF, which is generated from the electrolyte decomposition at a high cut-off voltage of 4.6V [33,34]. Layered Li-Ni-Co-Mn-O based material is also a widely applied commercial material. Till now, an LATP layer has been used as a surface layer in NCM811 [35] and NCM622 materials [36]. In this case, the effects of an LATP layer on the performance of NCM111 material is a worthy question to study. In this work, LATP was employed on the surface of NCM to alleviate surface side reactions. The LATP layer was prepared with a simple wet chemical method. It was found that the LATP-modified NCM exhibits an increased discharge capacity retention of 92.37% after 100 cycles at 0.2C, while the bare NCM only presents 64.28%. This result indicates that LATP-surface coating might be an effective method to increase the cycle stability of NCM at a high cut-off voltage of 4.6 V, which would improve the energy density of NCM in practical usage.

2. Experimental

2.1. Preparation of Materials

Commercial $\text{LiNi}_{1/3}\text{Co}_{1/3}\text{Mn}_{1/3}\text{O}_2$ (NCM) powder was used in this research. The $\text{Li}_{1.3}\text{Al}_{0.3}\text{Ti}_{1.7}(\text{PO}_4)_3$ -modified NCM samples (NCM@LATP) were synthesized by a wet chemical method, and the schematic diagram is shown in Figure 1. The precursors were LiNO_3 (99%), $\text{AlNO}_3 \cdot 9\text{H}_2\text{O}$ (AR), $\text{C}_{12}\text{H}_{28}\text{O}_4\text{Ti}$ (98%), and $\text{NH}_4\text{H}_2\text{PO}_4$ (98%). Typically, stoichiometric amounts of precursors were dissolved in a beaker, then commercial NCM was added in. The weight ratio of LATP was set to be 0.5 wt% (NCM@0.5LATP) and 1 wt% (NCM@1LATP), respectively. The mixture was heated and stirred for 8 h. When the solution was about to evaporate to dryness, it was put into an oven and dried at 60 °C to completely evaporate the remaining solvent. The collected powder was pre-heated at 300 °C for 3 h, and then sintered at 800 °C for 2 h to obtain the final sample.

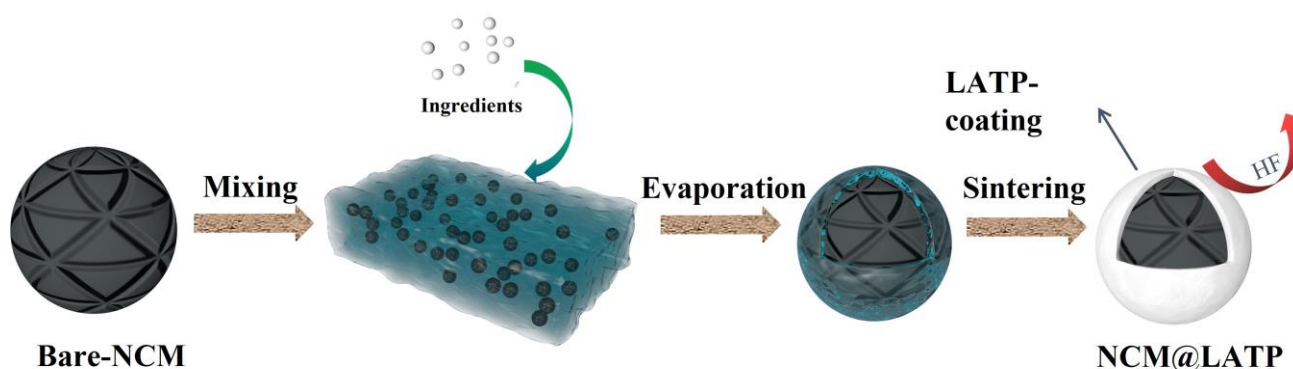


Figure 1. Schematic illustration for the LATP coating process.

2.2. Characterization of Materials

Crystalline structures of the samples were identified by X-ray diffraction (XRD, D8 Advance, Bruker, Karlsruhe, Germany). Scanning electron microscopy (SEM, Hitachi SU3500, Hitachi, Tokyo, Japan) was performed to check the morphology of the samples. Detailed morphological and lattice information were tested using a transmission electron microscopy instrument (TEM, Tecnai G2 F20, FEI, Eindhoven, The Netherlands). X-ray photoelectron spectroscope (XPS, Thermo Scientific K-Alpha, Waltham, MA, USA) was used to detect the surface composition. Surface area analyzer (ASAP2460, Micromeritics, Norcross, GA, USA) was used to obtain the N_2 adsorption/desorption isotherms.

2.3. Electrochemical Characterization

Electrochemical characterization was performed following earlier reports [34]. The cells were cycled between 2.5 and 4.6 V at a rate of 0.2C or 1C ($1C = 200 \text{ mA g}^{-1}$).

3. Results and Discussion

Figure 2 shows the XRD patterns of the two modified materials with different ratios (NCM@0.5LATP and NCM@1LATP) and the untreated material (bare NCM). All the diffraction peaks can be ascribed to the layered hexagonal α -NaFeO₂ type structure. The two obvious split peaks from (006)/(012) and (018)/(110) also infer that all three sample presents typical layered structures [37]. This means the structure of NCM remained unchanged after the treatment. According to the XRD results, no diffraction peaks of LATP were observed.

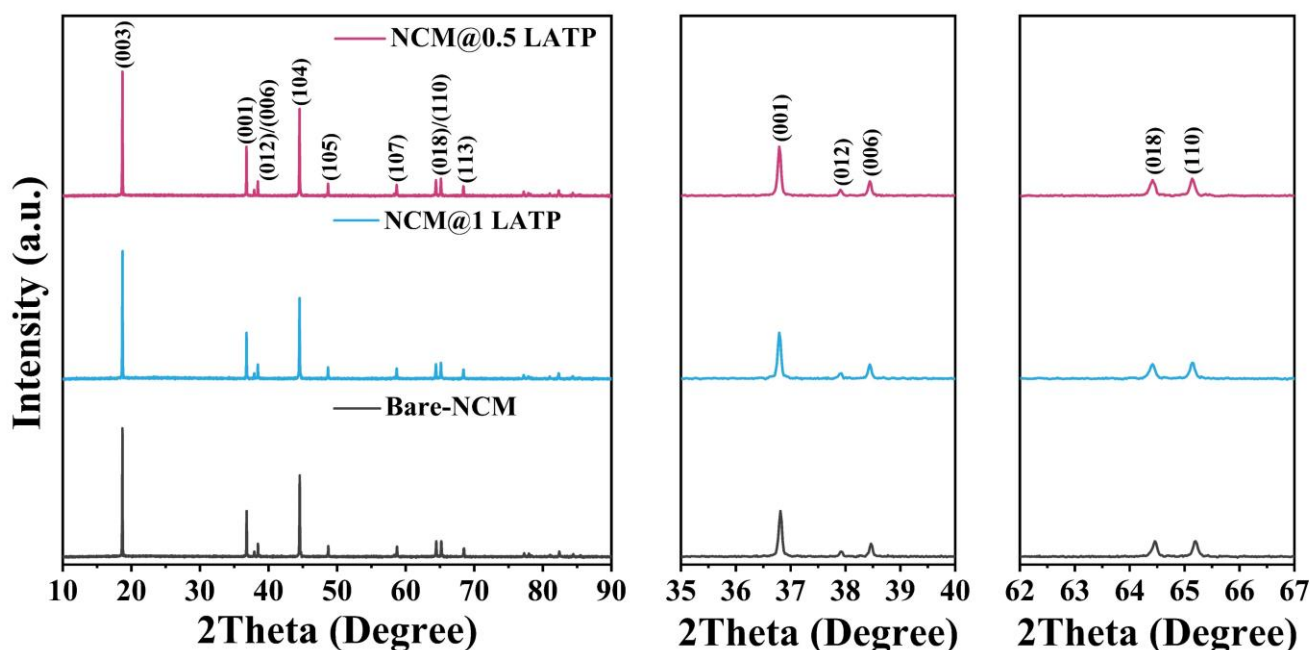


Figure 2. XRD patterns of bare NCM, NCM@0.5LATP, and NCM@1LATP.

Figure 3a–c show the SEM images of the three samples. According to the results, the bare NCM is basically uniform in size with a micron-level structure. The particles are in the shape of small spheres with good crystallization. Due to the relatively large size of the particles, it is difficult to see whether the coating is successful based on the particle morphology alone. In this case, NCM@0.5LATP was chosen for further study. EDS result confirms the existence of P, Al, and Ti elements in this sample. Elemental mapping results are shown in Figure 3e–k. It can be seen that the elements of Ni, Co, and Mn are distributed uniformly in the NCM@0.5LATP, and the shape of spherical particles can be clearly observed. By comparison, for the results of P, Al, and Ti, the spherical contour is not obvious. The reason may be that the coating layer is very thin and the element contents of P, Ti, and Al are very low. These results indicate that LATP exists on the surface of NCM particles.

To further demonstrate the existence of the LATP layer more intuitively, the surfaces of the bare NCM and NCM@0.5LATP samples were inspected by TEM. As illustrated in the TEM images shown in Figure 4a,b, clear lattice fringes can be observed up to the edge. The interplanar distance was calculated to be 0.23 nm, and it should be related to the (003) crystal plane. For the NCM@0.5LATP sample, an amorphous layer can be seen on the surface. This should be the LATP layer, which indicates LATP might coat on the surface in the amorphous form.

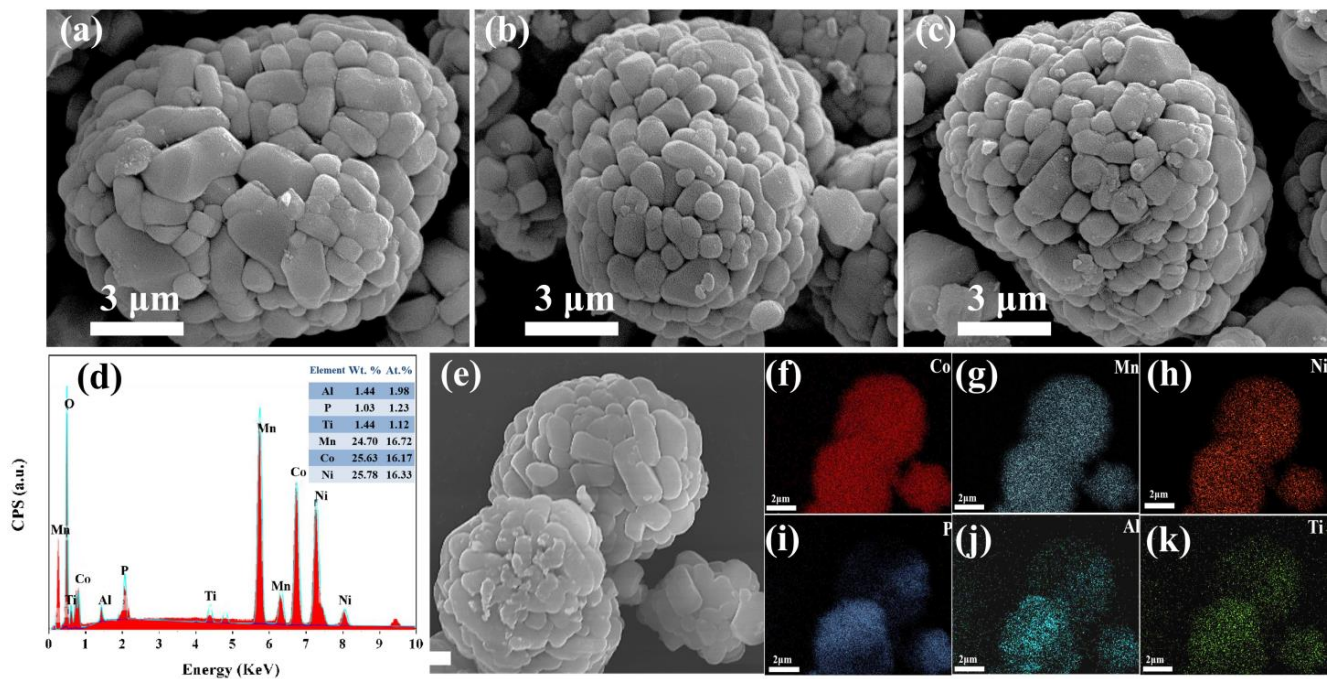


Figure 3. SEM images of (a) bare NCM, (b) NCM@0.5LTP, and (c) NCM@1LTP; (d) EDS spectrum; (e) area for the elemental mapping; elemental mapping of Co (f), Mn (g), Ni (h), P (i), Al (j), and Ti (k).

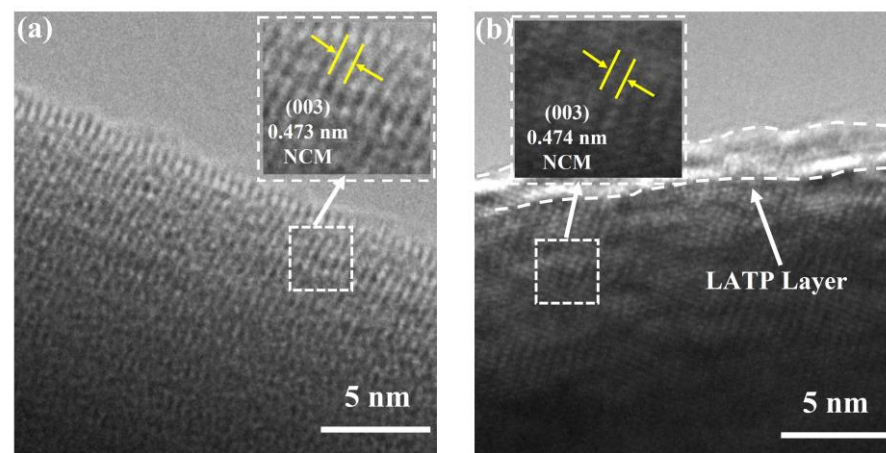


Figure 4. TEM images of (a) bare NCM and (b) NCM@0.5LTP.

Surface compositions of bare NCM and NCM@0.5LTP were analyzed with XPS. Firstly, the presence of characteristic peaks of Ni, Co, O, Mn, and C elements can be observed from the full spectrum of bare NCM, which is consistent with the previous EDS results. While for the NCM@0.5LTP sample, extra characteristic peaks of Al, Ti, and P are also observed in the spectrum. This result indicates that Al, Ti and P exist on the surface of NCM@0.5LTP. Figure 5b,c show the high-resolution XPS spectra of the P and Ti elements in the NCM@0.5LTP sample. Peaks at 458.3 eV and 463.9 eV can be ascribed to the binding energies of Ti 2p_{3/2} and Ti 2p_{1/2}, which correspond to Ti⁴⁺ ions in the Ti-based compounds [38]. Figure 5d–f show the high-resolution XPS spectra of the Co, Mn, and Ni elements. The peaks of the three elements are nearly the same in the bare NCM and NCM@0.5LTP samples, which indicates the valence states of Ni, Co, and Mn remained unchanged after the LTP modification [39].

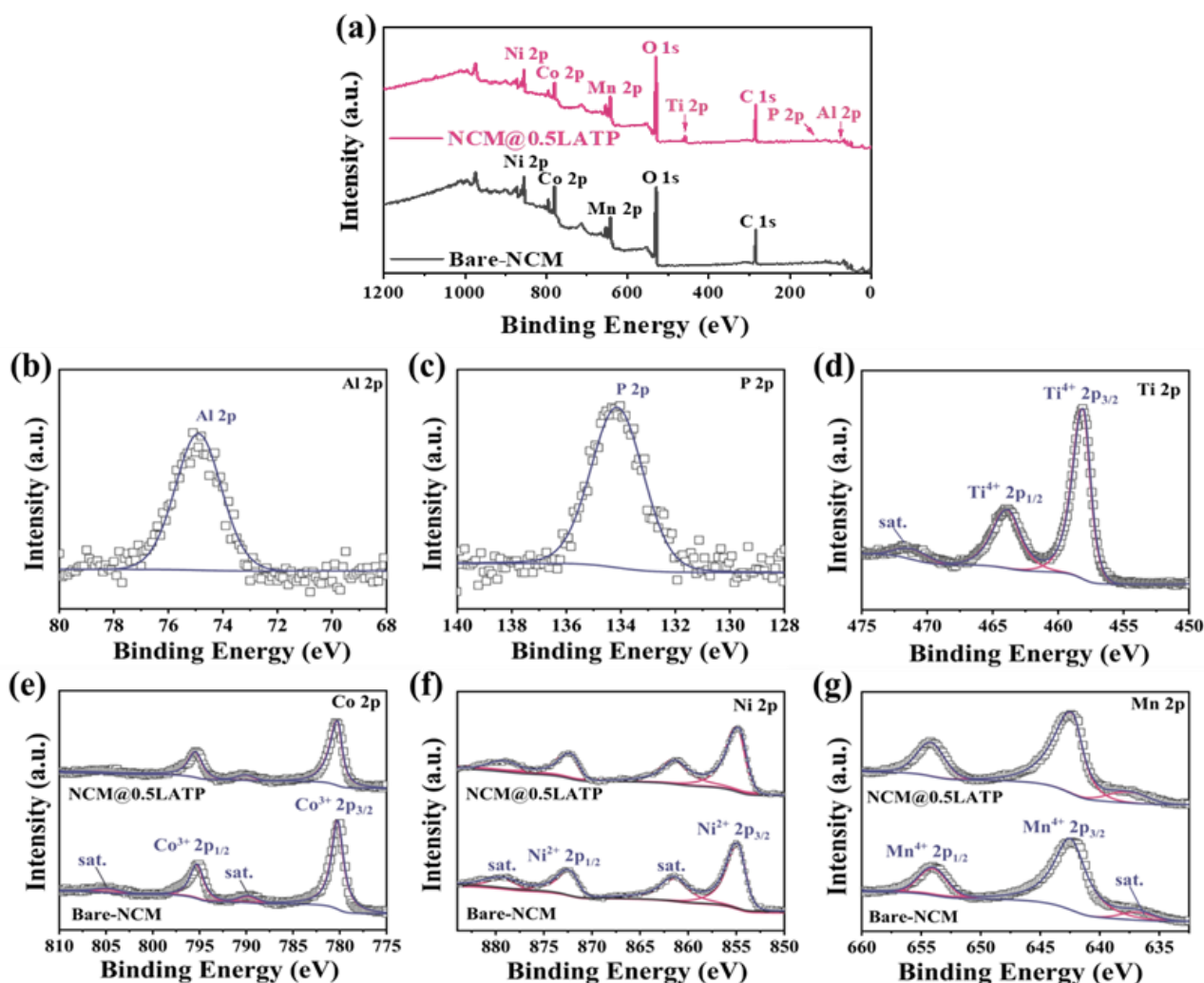


Figure 5. XPS spectra of (a) bare NCM and NCM@0.5LATP; high resolution spectra of (b) P 2p, (c) P 2p, (d) Ti 2p for NCM@0.5LATP, and (e) Co 2p, (f) Ni 2p, and (g) Mn 2p for bare NCM and NCM@0.5LATP.

Figure 6 shows the N_2 adsorption/desorption isotherms, and the shapes of the two samples are similar. However, for both samples, the end point of the desorption curve cannot match the start point of the adsorption curve. The reason may be the surface areas of two samples are relatively small [40,41]. Based on present data, the surface areas of bare NCM and NCM@0.5%LATP are calculated to be $\sim 4.7661 \text{ m}^2 \text{ g}^{-1}$ and $\sim 5.7378 \text{ m}^2 \text{ g}^{-1}$, respectively.

Galvanostatic charge–discharge and rate performances were tested for all three samples. For the bare NCM sample (Figure 7a), a significant declination in both voltage and capacity appears during the cycles. The reason is related to the HF corrosion of electrode materials by point decomposition at high voltage [42]. The discharge capacity of bare NCM drops to 122.4 mAh g^{-1} after 50 cycles at 0.2C, with a capacity retention of only 64.28%. The NCM@0.5LATP (Figure 7b) and NCM@1LATP (Figure 7c) samples share similar discharge curves and are both much better than the bare NCM. While the discharge capacity of NCM@0.5LATP is slightly larger than that of NCM@1LATP, which suggests the former sample presents a better performance at this rate. This result indicates that though LATP is a Li-ion conductor, a thick layer of LATP might decrease the conductivity of the electrode and degrade the discharge capacity [35,43–45]. Results in Figure 7e show that when the rate is increased to 1C, the discharge-specific capacities of all three sample materials decrease. The capacity decay of the bare NCM sample is more obvious than that

of the other samples. Figure 7f shows the rate performance of the three samples, and the chosen rates are 0.2C, 0.5C, 1C, 2C, and 5C, respectively. At small rates such as 0.2C, 0.5C, and 1C, the capacity of the bare NCM sample is larger than the other two samples, which is coincident with the cycle performances shown in Figure 7d,e. When the rate increases to 2C and 5C, the capacity of the bare NCM become much lower. At this time, the NCM@1LATP sample shows the largest capacity. It can still deliver a capacity of 70 mAh g⁻¹ at 5C. The above results indicate that NCM@0.5LATP exhibits the best cycling performance in the three samples at a cut-off voltage of 4.6 V. Earlier reports suggest some undesirable spinel phases grow during the cycles, and they will cause the decrease in voltage and capacity [46]. According to our results, the growth of spinel phase would be attenuated by the LATP layer, and the electrochemical performances are increased.

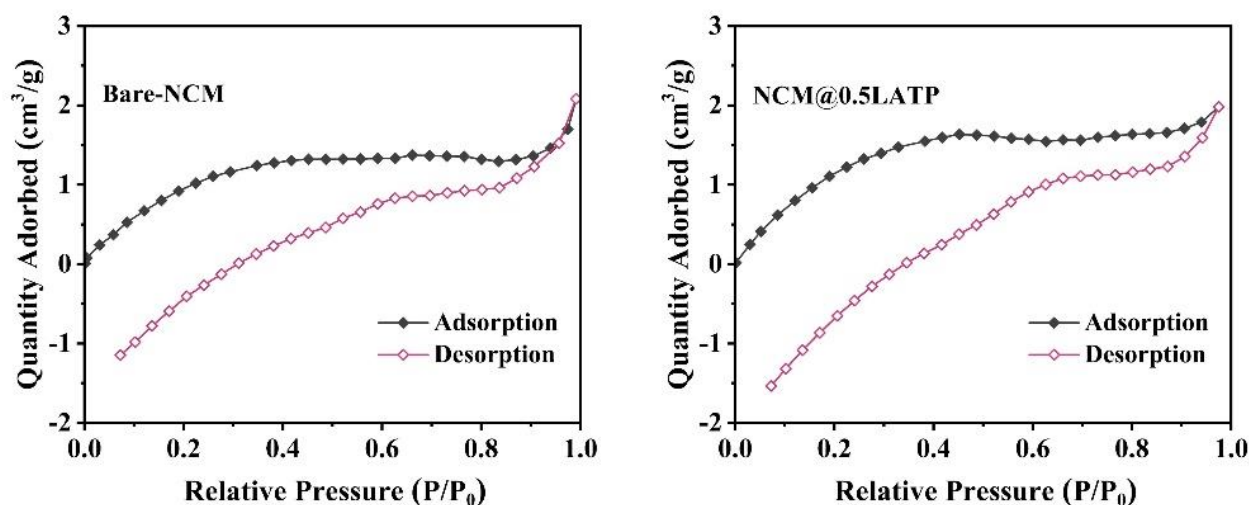


Figure 6. N₂ adsorption/desorption isotherms of bare NCM and NCM@0.5LATP.

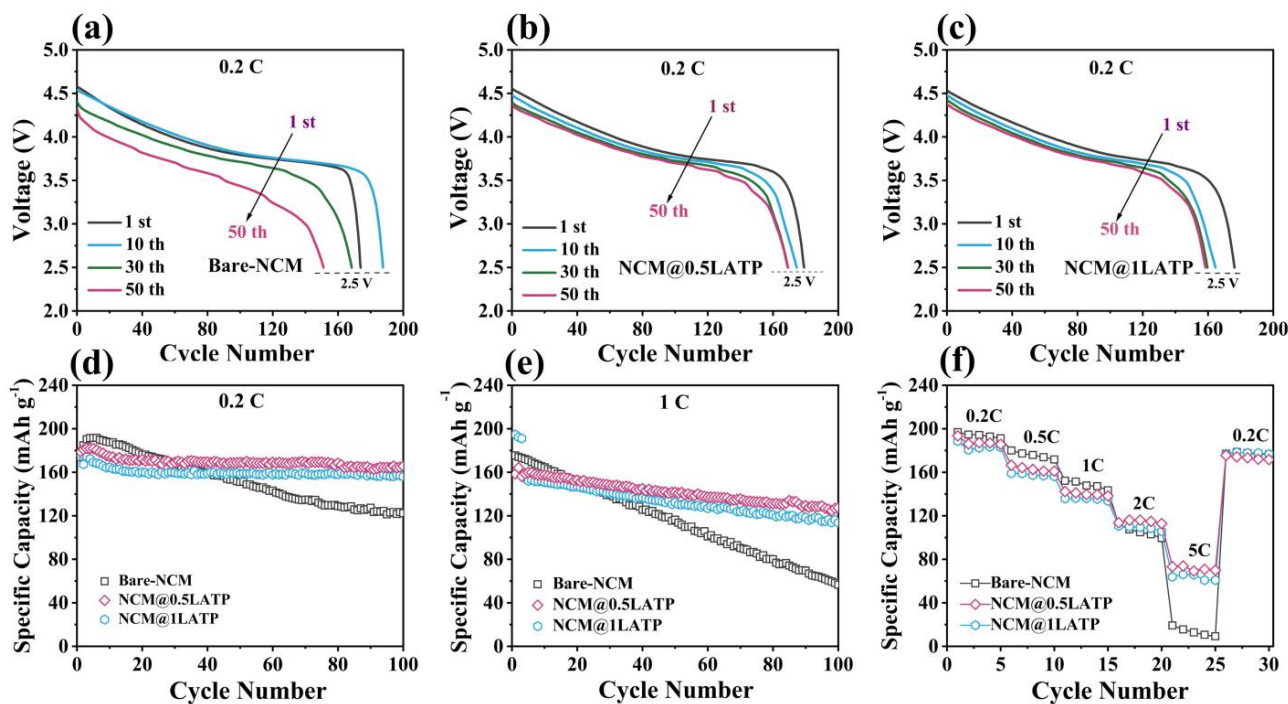


Figure 7. Discharge profiles of (a) bare NCM, (b) NCM@0.5LATP, and (c) NCM@1LATP; cycle performance of the three samples at (d) 0.2C and (e) 1C rate; (f) rate performances of the three samples.

To reveal the effect of the LAMP layer on the electrochemical internal resistances, EIS experiments were performed on bare NCM and NCM@0.5LAMP (Figure 8). The Nyquist curves of the two samples are similar. The equivalent circuit model used for fitting is shown in the inset. R1 in the model represents the Ohmic resistance, which may mainly come from the electrolyte, while R2 represents the charge transfer resistance. Table 1 shows the fitted parameters. According to the data, R2 of the bare NCM is 93.1 Ω before cycle, and increases to 146.7 Ω after 50 cycles, with a growth rate of 57.6%. While for NCM@0.5LAMP, R2 increases from 59.6 Ω to 75.3 Ω , with a growth rate of only 26.3%. This result indicates the surface layer of NCM@0.5LAMP is much stable than that of the bare NCM. The reason may be the protective layer prevents the side reactions of the electrolyte from occurring, and forms a stable cathode–electrolyte interphase, which provides a better microporous channel for lithium-ion diffusion [13,14].

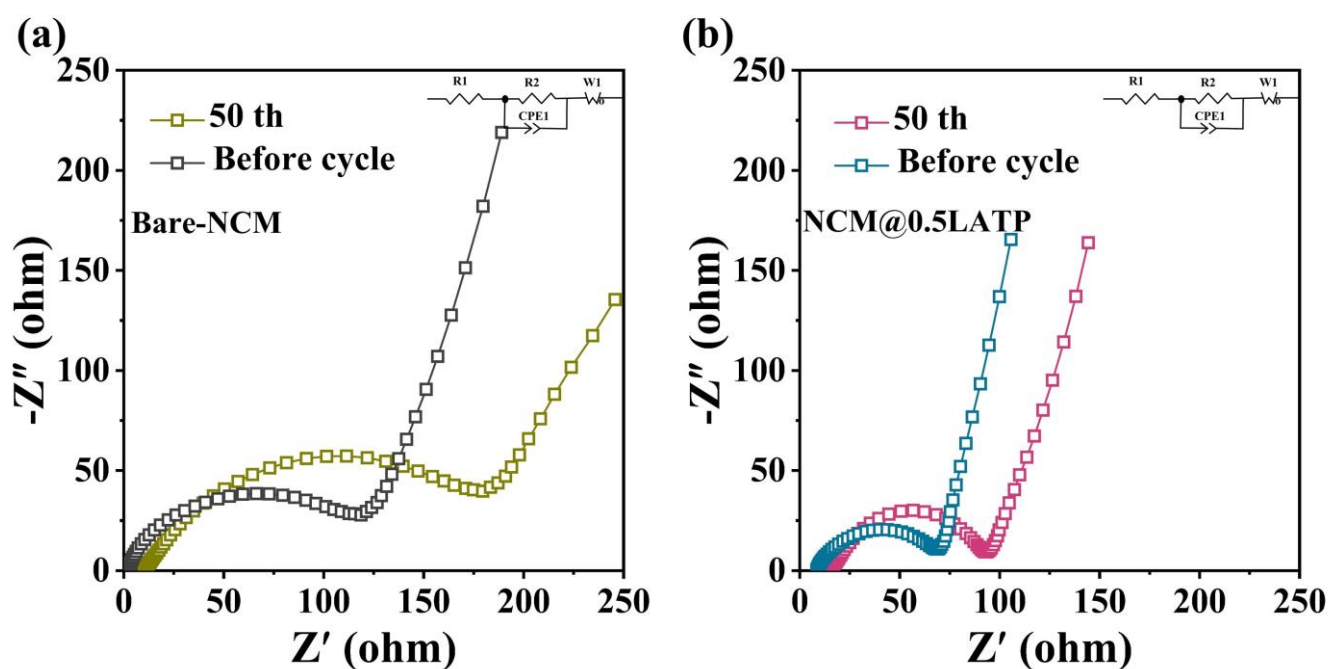


Figure 8. EIS results of (a) bare NCM and (b) NCM@0.5LAMP; inset is the used equivalent circuit model.

Table 1. Fitted impedance parameters.

Cycle Number	Before Cycle R ₂ (Ω)	50th Cycle R ₂ (Ω)
NCM@0.5LAMP	59.6	75.3
Bare-NCM	93.1	146.7

4. Conclusions

In summary, a homogeneous LAMP layer was prepared on an NCM surface by a simple wet chemical method. The sample with 0.5 wt% LAMP presents an increased capacity retention of 92.17% after 100 cycles at 0.2C. It also exhibits a better rate performance than the other two samples. EIS result indicates the surface layer of NCM@0.5LAMP is much stable than that of the bare NCM. Our results suggest that LAMP-surface coating might be an effective method to improve the cycle stability of NCM, and it might also be useful for other high-capacity cathode materials.

Author Contributions: Data curation, B.H.; Formal analysis, Y.G.; Investigation, M.Z.; Methodology, W.W.; Project administration, J.J.; Supervision, H.W.; Writing—original draft, P.Z.; Writing—review & editing, R.W. All authors have read and agreed to the published version of the manuscript.

Funding: This research was funded by Research on high power flexible battery in all sea depth (2020-XXXX-XX-246-00).

Institutional Review Board Statement: Not applicable.

Informed Consent Statement: Not applicable.

Conflicts of Interest: The authors declare no conflict of interests.

References

1. Kim, T.; Song, W.T.; Son, D.Y.; Ono, L.K.; Qi, Y.B. Lithium-ion batteries: Outlook on present, future, and hybridized technologies. *J. Mater. Chem. A* **2019**, *7*, 2942–2964. [[CrossRef](#)]
2. Liu, W.Y.; Yi, C.J.; Li, L.P.; Liu, S.L.; Gui, Q.Y.; Ba, D.L.; Li, Y.Y.; Peng, D.L.; Liu, J.P. Designing Polymer-in-Salt Electrolyte and Fully Infiltrated 3D Electrode for Integrated Solid-State Lithium Batteries. *Angew. Chem. Int. Ed.* **2021**, *60*, 12931–12940. [[CrossRef](#)] [[PubMed](#)]
3. Wang, R.; Li, X.; Liu, L.; Lee, J.; Seo, D.H.; Bo, S.H.; Urban, A.; Ceder, G. A disordered rock-salt Li-excess cathode material with high capacity and substantial oxygen redox activity: $\text{Li}_{1.25}\text{Nb}_{0.25}\text{Mn}_{0.5}\text{O}_2$. *Electrochem. Commun.* **2015**, *60*, 70–73. [[CrossRef](#)]
4. Wang, R.; He, X.Q.; He, L.H.; Wang, F.W.; Xiao, R.J.; Gu, L.; Li, H.; Chen, L.Q. Atomic Structure of Li_2MnO_3 after Partial Delithiation and Re-Lithiation. *Adv. Energy Mater.* **2013**, *3*, 1358–1367. [[CrossRef](#)]
5. Goodenough, J.B.; Park, K.S. The Li-Ion Rechargeable Battery: A Perspective. *J. Am. Chem. Soc.* **2013**, *135*, 1167–1176. [[CrossRef](#)] [[PubMed](#)]
6. Wang, R.; Yu, X.Q.; Bai, J.M.; Li, H.; Huang, X.J.; Chen, L.Q.; Yang, X.Q. Electrochemical decomposition of Li_2CO_3 in $\text{NiO-Li}_2\text{CO}_3$ nanocomposite thin film and powder electrodes. *J. Power Sources* **2012**, *218*, 113–118. [[CrossRef](#)]
7. Zhang, J.N.; Li, Q.H.; Ouyang, C.Y.; Yu, X.Q.; Ge, M.Y.; Huang, X.J.; Hu, E.Y.; Ma, C.; Li, S.F.; Xiao, R.J.; et al. Trace doping of multiple elements enables stable battery cycling of LiCoO_2 at 4.6V. *Nat. Energy* **2019**, *4*, 594–603. [[CrossRef](#)]
8. Liu, Z.L.; Yu, A.S.; Lee, J.Y. Synthesis and characterization of $\text{LiNi}_{1-x-y}\text{Co}_x\text{Mn}_y\text{O}_2$ as the cathode materials of secondary lithium batteries. *J. Power Sources* **1999**, *81*, 416–419. [[CrossRef](#)]
9. Chen, Y.; Zhao, W.M.; Zhang, Q.H.; Yang, G.Z.; Zheng, J.M.; Tang, W.; Xu, Q.J.; Lai, C.Y.; Yang, J.H.; Peng, C.X. Armoring $\text{LiNi}_{1/3}\text{Co}_{1/3}\text{Mn}_{1/3}\text{O}_2$ Cathode with Reliable Fluorinated Organic-Inorganic Hybrid Interphase Layer toward Durable High Rate Battery. *Adv. Funct. Mater.* **2020**, *30*, 2000396. [[CrossRef](#)]
10. Gao, A.; Sun, Y.; Zhang, Q.H.; Zheng, J.Y.; Lu, X. Evolution of Ni/Li antisites under the phase transition of a layered $\text{LiNi}_{1/3}\text{Co}_{1/3}\text{Mn}_{1/3}\text{O}_2$ cathode. *J. Mater. Chem. A* **2020**, *8*, 6337–6348. [[CrossRef](#)]
11. Lee, G.H.; Wu, J.P.; Kim, D.; Cho, K.; Cho, M.; Yang, W.L.; Kang, Y.M. Reversible Anionic Redox Activities in Conventional $\text{LiNi}_{1/3}\text{Co}_{1/3}\text{Mn}_{1/3}\text{O}_2$ Cathodes. *Angew. Chem. Int. Ed.* **2020**, *59*, 8681–8688. [[CrossRef](#)] [[PubMed](#)]
12. Song, Y.J.; Wang, M.R.; Li, J.; Cui, H.T.; Su, H.J.; Liu, Y.Y. Controllable synthesis of $\text{LiNi}_{1/3}\text{Co}_{1/3}\text{Mn}_{1/3}\text{O}_2$ electrode material via a high shear mixer-assisted precipitation process. *Chem. Eng. J.* **2021**, *419*, 129281. [[CrossRef](#)]
13. Hwang, B.J.; Tsai, Y.W.; Chen, C.H.; Santhanam, R. Influence of Mn content on the morphology and electrochemical performance of $\text{LiNi}_{1-x-y}\text{Co}_x\text{Mn}_y\text{O}_2$ cathode materials. *J. Mater. Chem.* **2003**, *13*, 1962–1968. [[CrossRef](#)]
14. Lee, K.S.; Myung, S.T.; Amine, K.; Yashiro, H.; Sun, Y.K. Structural and electrochemical properties of layered $\text{LiNi}_{1-2x}\text{Co}_x\text{Mn}_x\text{O}_2$ ($x=0.1-0.3$) positive electrode materials for Li-ion batteries. *J. Electrochem. Soc.* **2007**, *154*, A971–A977. [[CrossRef](#)]
15. Liu, X.P.; Chen, Q.Q.; Li, Y.W.; Chen, C.; Zeng, W.; Yuan, M.; Wang, R.H.; Xiao, S.H. Synergistic Modification of Magnesium Fluoride/Sodium for Improving the Electrochemical Performances of High-Nickel Ternary (NCM811) Cathode Materials. *J. Electrochem. Soc.* **2019**, *166*, A3480–A3486. [[CrossRef](#)]
16. Wu, K.; Li, Q.; Dang, R.B.; Deng, X.; Chen, M.M.; Lee, Y.L.; Xiao, X.L.; Hu, Z.B. A novel synthesis strategy to improve cycle stability of $\text{LiNi}_{0.8}\text{Mn}_{0.1}\text{Co}_{0.1}\text{O}_2$ at high cut-off voltages through core-shell structuring. *Nano Res.* **2019**, *12*, 2460–2467. [[CrossRef](#)]
17. Shi, C.G.; Shen, C.H.; Peng, X.X.; Luo, C.X.; Shen, L.F.; Sheng, W.J.; Fan, J.J.; Wang, Q.; Zhang, S.J.; Xu, B.B.; et al. A special enabler for boosting cyclic life and rate capability of $\text{LiNi}_{0.8}\text{Co}_{0.1}\text{Mn}_{0.1}\text{O}_2$: Green and simple additive. *Nano Energy* **2019**, *65*, 104084. [[CrossRef](#)]
18. Yoon, T.; Soon, J.; Lee, T.J.; Ryu, J.H.; Oh, S.M. Dissolution of cathode-electrolyte interphase deposited on $\text{LiNi}_{0.5}\text{Mn}_{1.5}\text{O}_4$ for lithium-ion batteries. *J. Power Sources* **2021**, *503*, 230051. [[CrossRef](#)]
19. Zhang, J.N.; Li, Q.H.; Wang, Y.; Zheng, J.Y.; Yu, X.Q.; Li, H. Dynamic evolution of cathode electrolyte interphase (CEI) on high voltage LiCoO_2 cathode and its interaction with Li anode. *Energy Storage Mater.* **2018**, *14*, 1–7. [[CrossRef](#)]
20. Zhao, J.T.; Liang, Y.; Zhang, X.; Zhang, Z.H.; Wang, E.R.; He, S.M.; Wang, B.Y.; Han, Z.J.; Lu, J.; Amine, K.; et al. In Situ Construction of Uniform and Robust Cathode-Electrolyte Interphase for Li-Rich Layered Oxides. *Adv. Funct. Mater.* **2021**, *31*, 2009192. [[CrossRef](#)]
21. Hossain, M.K.; Raihan, G.A.; Akbar, M.A.; Kabir Rubel, M.H.; Ahmed, M.H.; Khan, M.I.; El-Denglawey, A. Current Applications and Future Potential of Rare Earth Oxides in Sustainable Nuclear, Radiation, and Energy Devices: A Review. *ACS Appl. Electron. Mater.* **2022**, *4*, 3327. [[CrossRef](#)]
22. Li, Z.C.; Zhang, Z.H.; Huang, B.J.; Wang, H.W.; He, B.B.; Gong, Y.S.; Jin, J.; Wang, R. Improved Cycling Performance of Cation-Disordered Rock-Salt $\text{Li}_{1.2}\text{Ti}_{0.4}\text{Mn}_{0.4}\text{O}_2$ Cathode through Mo-Doping and Al_2O_3 -Coating. *Coatings* **2022**, *12*, 1613. [[CrossRef](#)]

23. Yang, C.F.; Zhang, X.S.; Huang, M.Y.; Huang, J.J.; Fang, Z.B. Preparation and Rate Capability of Carbon Coated $\text{LiNi}_{1/3}\text{Co}_{1/3}\text{Mn}_{1/3}\text{O}_2$ as Cathode Material in Lithium Ion Batteries. *ACS Appl. Mater. Interfaces* **2017**, *9*, 12408–12415. [[CrossRef](#)] [[PubMed](#)]
24. Wang, J.H.; Wang, Y.; Guo, Y.Z.; Liu, C.W.; Dan, L.L. Electrochemical characterization of AlPO_4 coated $\text{LiNi}_{1/3}\text{Co}_{1/3}\text{Mn}_{1/3}\text{O}_2$ cathode materials for high temperature lithium battery application. *Rare Metals* **2021**, *40*, 78–83. [[CrossRef](#)]
25. Ren, X.Y.; Du, J.L.; Pu, Z.H.; Wang, R.B.; Gan, L.; Wu, Z. Facile synthesis of Li_2MoO_4 coated $\text{LiNi}_{1/3}\text{Co}_{1/3}\text{Mn}_{1/3}\text{O}_2$ composite as a novel cathode for high-temperature lithium batteries. *Ionics* **2020**, *26*, 1617–1627. [[CrossRef](#)]
26. Li, J.H.; Liu, Z.Q.; Wang, Y.F.; Wang, R.G. Investigation of facial B_2O_3 surface modification effect on the cycling stability and high-rate capacity of $\text{LiNi}_{1/3}\text{Co}_{1/3}\text{Mn}_{1/3}\text{O}_2$ cathode. *J. Alloys Compd.* **2020**, *834*, 155150. [[CrossRef](#)]
27. Araki, K.; Taguchi, N.; Sakaebe, H.; Tatsumi, K.; Ogumi, Z. Electrochemical properties of $\text{LiNi}_{1/3}\text{Co}_{1/3}\text{Mn}_{1/3}\text{O}_2$ cathode material modified by coating with Al_2O_3 nanoparticles. *J. Power Sources* **2014**, *269*, 236–243. [[CrossRef](#)]
28. Ilango, P.R.; Subburaj, T.; Prasanna, K.; Jo, Y.N.; Lee, C.W. Physical and electrochemical performance of $\text{LiNi}_{1/3}\text{Co}_{1/3}\text{Mn}_{1/3}\text{O}_2$ cathodes coated by Sb_2O_3 using a sol-gel process. *Mater. Chem. Phys.* **2015**, *158*, 45–51. [[CrossRef](#)]
29. Lv, F.; Cheng, H.W.; Nie, W.; Sun, Q.C.; Liu, Y.B.; Duan, T.; Xu, Q.; Lu, X.G. Enhancing Rate Capacity and Cycle Stability of $\text{LiNi}_{1/3}\text{Co}_{1/3}\text{Mn}_{1/3}\text{O}_2$ Cathode Material by Laminar V_2O_5 Coating for Lithium-Ion Batteries. *Chemistryselect* **2021**, *6*, 6339–6347. [[CrossRef](#)]
30. Monchak, M.; Hupfer, T.; Senyshyn, A.; Boysen, H.; Chernyshov, D.; Hansen, T.; Schell, K.G.; Bucharsky, E.C.; Hoffmann, M.J.; Ehrenberg, H. Lithium Diffusion Pathway in $\text{Li}_{1.3}\text{Al}_{0.3}\text{Ti}_{1.7}(\text{PO}_4)_3$ (LATP) Superionic Conductor. *Inorg. Chem.* **2016**, *55*, 2941–2945. [[CrossRef](#)]
31. DeWees, R.; Wang, H. Synthesis and Properties of NaSICON-type LATP and LAGP Solid Electrolytes. *ChemSuschem* **2019**, *12*, 3713–3725. [[CrossRef](#)] [[PubMed](#)]
32. Zhao, E.Q.; Ma, F.R.; Jin, Y.C.; Kanamura, K. Pechini synthesis of high ionic conductivity $\text{Li}_{1.3}\text{Al}_{0.3}\text{Ti}_{1.7}(\text{PO}_4)_3$ solid electrolytes: The effect of dispersant. *J. Alloys Compd.* **2016**, *680*, 646–653. [[CrossRef](#)]
33. Kalluri, S.; Yoon, M.; Jo, M.; Liu, H.K.; Dou, S.X.; Cho, J.; Guo, Z.P. Feasibility of Cathode Surface Coating Technology for High-Energy Lithium-ion and Beyond-Lithium-ion Batteries. *Adv. Mater.* **2017**, *29*, 1605807. [[CrossRef](#)] [[PubMed](#)]
34. Qu, Z.T.; Liu, S.T.; Zhang, P.; Wang, R.; Wang, H.W.; He, B.B.; Gong, Y.S.; Jin, J.; Li, S. Enhanced electrochemical performances of LiCoO_2 at high cut-off voltage by introducing LiF additive. *Solid State Ion.* **2021**, *365*, 115654. [[CrossRef](#)]
35. Kim, M.-Y.; Song, Y.-W.; Lim, J.; Park, S.-J.; Kang, B.-S.; Hong, Y.; Kim, H.-S.; Han, J.H. LATP-coated NCM-811 for high-temperature operation of all-solid lithium battery. *Mater. Chem. Phys.* **2022**, *290*, 126644. [[CrossRef](#)]
36. Song, G.W.; Zhong, H.; Wang, Z.; Dai, Y.Y.; Zhou, X.Y.; Yang, J. Interfacial Film $\text{Li}_{1.3}\text{Al}_{0.3}\text{Ti}_{1.7}\text{PO}_4$ -Coated $\text{LiNi}_{0.6}\text{Co}_{0.2}\text{Mn}_{0.2}\text{O}_2$ for the Long Cycle Stability of Lithium-Ion Batteries. *ACS Appl. Energy Mater.* **2019**, *2*, 7923. [[CrossRef](#)]
37. Kobylanska, S.; Demchuk, D.; Khomenko, V.; Barsukov, V.; Belous, A. Surface Modification of the $\text{LiNi}_{0.5}\text{Co}_{0.2}\text{Mn}_{0.3}\text{O}_2$ Cathode by a Protective Interface Layer of $\text{Li}_{1.3}\text{Ti}_{1.7}\text{Al}_{0.3}(\text{PO}_4)_3$. *J. Electrochem. Soc.* **2019**, *166*, A1920–A1925. [[CrossRef](#)]
38. Jin, Y.M.; Zong, X.; Zhang, X.B.; Liu, C.J.; Li, D.; Jia, Z.G.; Li, G.; Zhou, X.G.; Wei, J.H.; Xiong, Y.P. Interface regulation enabling three-dimensional $\text{Li}_{1.3}\text{Al}_{0.3}\text{Ti}_{1.7}(\text{PO}_4)_3$ -reinforced composite solid electrolyte for high-performance lithium batteries. *J. Power Sources* **2021**, *501*, 230027. [[CrossRef](#)]
39. Huang, B.J.; Wang, R.; Gong, Y.S.; He, B.B.; Wang, H.W. Enhanced Cycling Stability of Cation Disordered Rock-Salt $\text{Li}_{1.2}\text{Ti}_{0.4}\text{Mn}_{0.4}\text{O}_2$ Material by Surface Modification with Al_2O_3 . *Front. Chem.* **2019**, *7*, 107. [[CrossRef](#)]
40. Kamiyama, A.; Kubota, K.; Nakano, T.; Fujimura, S.; Shiraiishi, S.; Tsukada, H.; Komaba, S. High-Capacity Hard Carbon Synthesized from Macroporous Phenolic Resin for Sodium-Ion and Potassium-Ion Battery. *ACS Appl. Energy Mater.* **2020**, *3*, 135. [[CrossRef](#)]
41. Kubota, K.; Shimadzu, S.; Yabuuchi, N.; Tominaka, S.; Shiraiishi, S.; Abreu-Sepulveda, M.; Manivannan, A.; Gotoh, K.; Fukunishi, M.; Dahbi, M.; et al. Structural Analysis of Sucrose-Derived Hard Carbon and Correlation with the Electrochemical Properties for Lithium, Sodium, and Potassium Insertion. *Chem. Mater.* **2020**, *32*, 2961. [[CrossRef](#)]
42. Nie, K.H.; Sun, X.R.; Wang, J.Y.; Wang, Y.; Qi, W.B.; Xiao, D.D.; Zhang, J.N.; Xiao, R.J.; Yu, X.Q.; Li, H.; et al. Realizing long-term cycling stability and superior rate performance of 4.5 V- LiCoO_2 by aluminum doped zinc oxide coating achieved by a simple wet-mixing method. *J. Power Sources* **2020**, *470*, 228423. [[CrossRef](#)]
43. Myung, S.-T.; Amine, K.; Sun, Y.-K. Surface modification of cathode materials from nano- to microscale for rechargeable lithium-ion batteries. *J. Mater. Chem.* **2010**, *20*, 7074. [[CrossRef](#)]
44. Sari, H.M.K.; Li, X. Controllable Cathode-Electrolyte Interface of $\text{Li}[\text{Ni}_{0.8}\text{Co}_{0.1}\text{Mn}_{0.1}]\text{O}_2$ for Lithium Ion Batteries: A Review. *Adv. Energy Mater.* **2019**, *9*, 1901597. [[CrossRef](#)]
45. Chen, Z.; Qin, Y.; Amine, K.; Sun, Y.K. Role of surface coating on cathode materials for lithium-ion batteries. *J. Mater. Chem.* **2010**, *20*, 7606. [[CrossRef](#)]
46. Li, Q.; Li, G.S.; Fu, C.C.; Luo, D.; Fan, J.M.; Li, L.P. K^+ -Doped $\text{Li}_{1.2}\text{Mn}_{0.54}\text{Co}_{0.13}\text{Ni}_{0.13}\text{O}_2$: A Novel Cathode Material with an Enhanced Cycling Stability for Lithium-Ion Batteries. *ACS Appl. Mater. Interfaces* **2014**, *6*, 10330–10341. [[CrossRef](#)]